A facile salt-templating synthesis route of bamboo-derived hierarchical porous carbon for supercapacitor applications

Tan Binh Nguyen [a], Bumyong Yoon [a], Trong Danh Nguyen [b], Eunyoung Oh [c], Yifei Ma [d], Mei Wang [d], Jonghwan Suhr [a,c,*]

[a] Department of Polymer Science and Engineering, Sungkyunkwan University, Suwon-si, 16419, Republic of Korea
[b] Department of Materials Science and Engineering, Gachon University, 1342 Seongnam-Daero, Sujeong-Gu, Seongnam-si, 13120, Republic of Korea
[c] School of Mechanical Engineering, Sungkyunkwan University, Suwon-si, 16419, Republic of Korea
[d] Institute of Laser Spectroscopy, Shanxi University, Taiyuan, 030006, China

ARTICLE INFO

ABSTRACT

Porous carbon materials have been widely used as electrodes for various energy storage and conversion devices, particularly for supercapacitors. Herein, a bamboo-derived hierarchical porous carbon (BHPC) is directly prepared under air atmosphere via an eco-friendly, one-step, and easily-scalable salt-templating strategy using ZnCl$_2$/KCl salt mixture as a pore-directing solvent. The obtained BHPC material exhibits large specific surface area (1296 m^2 g^{-1}) and large total pore volume (1.26 cm^3 g^{-1}) which make the BHPC material applicable for supercapacitor as an electrode material. Electrochemical performance evaluated in a 6 M KOH electrolyte in a three-electrode system indicates a high specific capacitance of 394 F g^{-1} at 1 A g^{-1} and a good rate capacity with 76.14% capacitance retention at 20 A g^{-1}. The as-prepared symmetric supercapacitor delivers a high energy density of 11 Wh kg^{-1} at a powder density of 126 W kg^{-1}, and an outstanding lifespan with 81% capacitance retention over 10,000 cycles. These results further open new possibilities for tailoring the surface properties (i.e., heteroatom doping, surface modification, metal oxides incorporation, etc.) towards energy storage and conversion applications such as electrocatalysts for oxygen reduction reaction/hydrogen evolution reaction, lithium-ion batteries, and supercapacitors, as well as wastewater treatment, and electromagnetic wave absorption applications.

1. Introduction

With the rapid development of global population, economy, and living standard, an ever-alarming increase in energy consumption is inevitable [1,2]. The uncontrollable energy utilization for unnecessary purposes directly links to the emerging of global warming, environmental pollution, and depletion of fossil fuels, resulting in an urgent call to produce energy from green, renewable, and sustainable sources instead of fossil fuels [3]. Tremendous efforts have been pursued to acquire energy from carbon dioxide-neutral and intermittent sources such as solar, wind, and tide, as well as to develop new technologies associated with efficient storing, converting, and using the above-mentioned energy sources [4,5]. Among various energy storage and conversion devices, supercapacitors (SCs) have been currently appealing considerable attention due to their high power density, long lifespan, fast charge-discharge rate, low maintenance cost, and environmental friendliness. Along with batteries, the SCs play an important role in many energy storage and conversion systems [6]. It has been critically concerned to design high-quality nanostructured electrode materials with large ion-accessible sites, high electrical conductivity, hierarchical porous architecture, and high electrochemical stability in order to obtain high-performance SCs devices [7]. In this regard, numerous carbon-based electrode materials for SCs have been explored, for example, carbon nanotubes, carbon nanofibers, mesoporous carbons, activated carbons, and graphene. Yet, the most common precursors of carbon-based materials are all derived from fossil fuels, such as coal, petroleum pitch, and asphalt [8]. Moreover, the current synthesis routes for the carbon-based materials are disadvantageous because of the complicated equipment, complex pre-synthesis and post-treatment, and the release of environmentally harmful byproducts after removal of

---

* Corresponding author. Department of Polymer Science and Engineering, School of Mechanical Engineering, Sungkyunkwan University, Suwon-si, 16419, Republic of Korea.
E-mail address: suhr@skku.edu (J. Suhr).

several hard templates [9]. Such issues put intense pressure on seeking for renewable carbon sources, along with developing green and facile synthesis procedures to meet the requirements for a long-term development of sustainable economy, society, and environment [10].

In the recent years, the intensive use of biomass in various applications is a key factor driving the growth of an environmentally sustainable society due to their natural abundance, renewability, and eco-friendliness. Moreover, the original building blocks of these natural biomaterials inherently possess unique and self-assembly nano-structures, which makes them suitable for preparing porous carbon as electrode material in SCs [11]. Among various biomass materials, bamboo is one of the fastest growing plants in the world, which is mainly distributed in the Asian region [12]. Bamboo charcoal (BC) is one of the most widely used products derived from the carbonization of bamboo and its residues under nitrogen atmosphere. Emerging as a low-cost material with naturally large surface area and porous structure, researchers have paid extensive attention for using BC in potential applications, such as absorbent for wastewater treatment, electromagnetic interference shielding and microwave absorption, and reinforcement for polymer composites[13–18]. However, the obtained BC mainly exhibits the undeveloped porosity (particularly micropores) with very low pore volume, which hindered its use in energy storage and conversion devices and is not applicable for high-performance SCs [19]. Moreover, seeking alternative synthesis strategies to develop new hierarchical porous carbon from bamboo compared to conventional bamboo charcoal have been rarely investigated. Multiple approaches have been conducted to produce porous carbon materials from biomass feedstocks. Classically, the conventional methods inevitably involve the etching of carbon atoms at high temperature using oxidant agents such as gases (CO_2, H_2O, or O_2) or solids (KOH, K_2CO_3, H_3PO_4, etc.) [20]. However, microporous carbon materials obtained from the above-mentioned approaches hinders the mass transport through the materials and thus lowering the electrochemical performance. On the other hand, templating methods have been adopted to obtain carbon materials with well-defined pore characteristic and controllable pore size and shape. Worse still, the conventional templating methods requires complicated pre-synthesis and post-treatment, which are the preparation and utilization of ordered hard templates, and the removal of those templates via acidic washing, resulting in the difficulty in commercial production and the conflict with sustainable development [21,22]. Therefore, the development of green and facile synthesis techniques to produce carbon materials with hierarchical porous structure, satisfying all requirements for high-performance SCs is indispensable.

In this study, a very simple, green, and cost-effective strategy is introduced to fabricate hierarchical porous carbon materials from bamboo as a renewable precursor. Instead of directly using bamboo charcoal with poor porosity, it was found that the $ZnCl_2$/KCl salt mixture applied in the carbonization shows a synergistic effect working as a solvent, protecting the materials from burning, and a template, designing the highly porous morphology structure. The carbonization process was operated in a muffle furnace under air atmosphere, without using sophisticated equipment and the inert gases. In addition, the $ZnCl_2$/KCl salt mixture was not directly involved in the carbonization reaction and can be easily removed by aqueous washing. To be endowed with superior characteristics such as large specific surface area, highly developed three-dimensional (3D) interconnected micro-meso-macroporous structure, and oxygenated functionalities, the obtained porous carbon materials were employed as electrodes for SCs, showing high specific capacitance, good rate performance, stable cycle life, high energy density, and powder density.

2. Experimental

2.1. Materials and reagents

Bamboo powder was provided by Hanyang Advanced Materials (South Korea). Zinc chloride ($ZnCl_2$, >98.0%, extra pure), potassium chloride (KCl, >99.0%, extra pure), potassium hydroxide (KOH, >93.0%, extra pure), and hydrochloride acid (HCl, 35.0–37.0%, guaranteed) were purchased from Daejung Chemical & Metals (South Korea). Super P carbon black (conductive, 99+%), *N*-methyl-2-pyrrolidone (NMP, 99.0+%, ACS grade) were obtained from Alfa Aesar by Thermo Fisher Scientific (USA). Poly (vinylidene difluoride) (PVDF, average Mw ~534,000 by GPC, powder) was supplied by Sigma-Aldrich (USA). Stainless-steel mesh was supplied by Seongho Sigma (South Korea). All materials and reagents were used as received.

2.2. Synthesis of bamboo-derived hierarchical porous carbon

The $ZnCl_2$ and KCl salts were mixed with a molar ratio of 54:46 to have 30 g of salt mixture. The salt mixture was blended with bamboo powder (3 g) as a carbon precursor in an agate mortar. Then the mixture was transferred to a porcelain crucible with a cover and then put into a muffle furnace. The carbonization process was conducted in the furnace under air atmosphere with a heating rate of 5 °C/min. Typically, the mixture was heated from room temperature to 250 °C and maintained at this temperature for 2 h. The temperature was then increased to 800 °C and the mixture was annealed at this temperature for 1 h. After the furnace chamber was allowed to cool down to room temperature, the materials were dispersed in 200 mL of 2 M HCl solution and stirred overnight to eliminate all the unreacted salts. The obtained black-colored product was collected after filtration through a 0.22 μm hydrophilic PVDF membrane (Sigma-Aldrich, USA) by an electric aspirator. The samples were undergone a washing process with 200 mL of 2 M HCl and 2000 mL of deionized water, respectively, and then finalized after vacuum-drying at 60 °C in a convection oven for 24 h. For comparison, samples were synthesized at different temperatures (500–900 °C) via the above-mentioned process, namely BHPC-X (X stands for annealing temperature). The sample directly pyrolyzed at 800 °C without the salt mixture was denoted as bamboo charcoal (BC-800).

2.3. Material characterization

The structural morphologies of the samples were examined by field emission scanning electron microscopy (FE-SEM, JSM−7600F, JEOL, Japan) at an accelerating voltage of 15 kV. Field emission transmission electron microscope (FE-TEM) micrographs were observed by FE-TEM (JEM−2100F, JEOL, Japan) at an accelerating voltage of 200 kV. Thermogravimetric analysis (TGA) was measured using a Q50 Universal V20.13 Build 39 (TA instruments, USA). All samples were heated from 30 to 800 °C at a heating rate of 5 °C/min under air atmosphere. Fourier-transform infrared (FTIR) spectra were recorded using an IFS−66/S, TENSOR27 instrument (Bruker, Germany) in the scanning wavenumber region from 400 to 4000 cm^{-1}, with a resolution of 4 cm^{-1}. Raman spectra were recorded using an Xper Raman instrument (Alvatek, UK) with a 532 nm excitation source. X-ray diffraction (XRD) were performed on a D8 ADVANCE instrument (Bruker, Germany) equipped with Cu Kα radiation (λ = 1.5406 Å) at an accelerating voltage of 40 kV and an operating current of 100 mA. X-ray photoelectron spectroscopy (XPS) was obtained by using an ESCALAB250 instrument (Thermo Fisher Scientific, UK) with Al Kα X-ray radiation source (1486.6 eV). Nitrogen adsorption/desorption measurements were implemented to obtain quantitative surface area and pore structural information about the samples using a surface area and porosity analyzer (TriStar II Plus Version 3.02, Micromeritics, USA). The samples were degassed at 150 °C under vacuum for 10 h before measurements. The specific surface area (SSA) of the samples was calculated from the nitrogen adsorption/desorption isotherm curves by the multi-point Brunauer-Emmett-Teller (BET) method. The pore size distribution (PSD), total pore volume (TPV), and micropore volume of the samples were extracted from the isotherms by the Barret-Joyner-Halenda (BJH) model.

2.4. Electrochemical measurement

The electrochemical properties of the obtained BHPC electrodes in a three-electrode system using 6 M KOH as an electrolyte were measured by a ZIVE SP1 electrochemical workstation. A platinum wire and Hg/HgO were served as the counter electrode and reference electrode, respectively. The working electrode was prepared by homogeneously mixing 90 wt% BHPC, 5 wt% Super P carbon black, and 5 wt% PVDF binder in NMP. The electrode material was painted on the current collector of stainless-steel mesh and dried at 80 °C for 24 h. Cyclic voltammetry (CV) tests were conducted in the operating voltage of − 1 V and 0 V (vs Hg/HgO) at different scan rates. Galvanostatic charge/discharge (GCD) tests were carried out at different current densities. Electrochemical impedance spectroscopy (EIS) was recorded in the frequency range of 100 kHz and 0.1 Hz with a 5 mV voltage amplitude. The same two electrodes separated by a porous membrane were assembled as the symmetric supercapacitor and tested in a two-electrode system using a battery test system WBCS3000S.

The gravimetric specific capacitance of a single electrode in a three-electrode system and a supercapacitor in a two-electrode system was calculated by using the following equations:

$$C_g = I\Delta t / m\Delta V, \tag{1}$$

$$C_g = 4I\Delta t / m\Delta V, \tag{2}$$

where I, Δt, m, and ΔV are the constant current (mA), discharging time (s), mass of one electrode in three-electrode system and both electrodes in two-electrode system (mg), and the operating voltage (V), respectively.

In the symmetric supercapacitor, the energy density (E, Wh kg^{-1}) and power density (P, W kg^{-1}) were calculated by the following equations:

$$E = C_g \Delta V^2 / 28.8, \tag{3}$$

$$P = 3600E / \Delta t, \tag{4}$$

3. Results and discussion

3.1. Structural and morphological characterization

The photographs shown in Fig. 1a indicate that the obtained BC-800 without using the ZnCl$_2$/KCl mixture presents the collapsed structure, whereas the BHPC-800 sample exhibits the self-standing and highly porous structures. During the direct carbonization under air atmosphere, the raw biomass material is converted into char with compacted
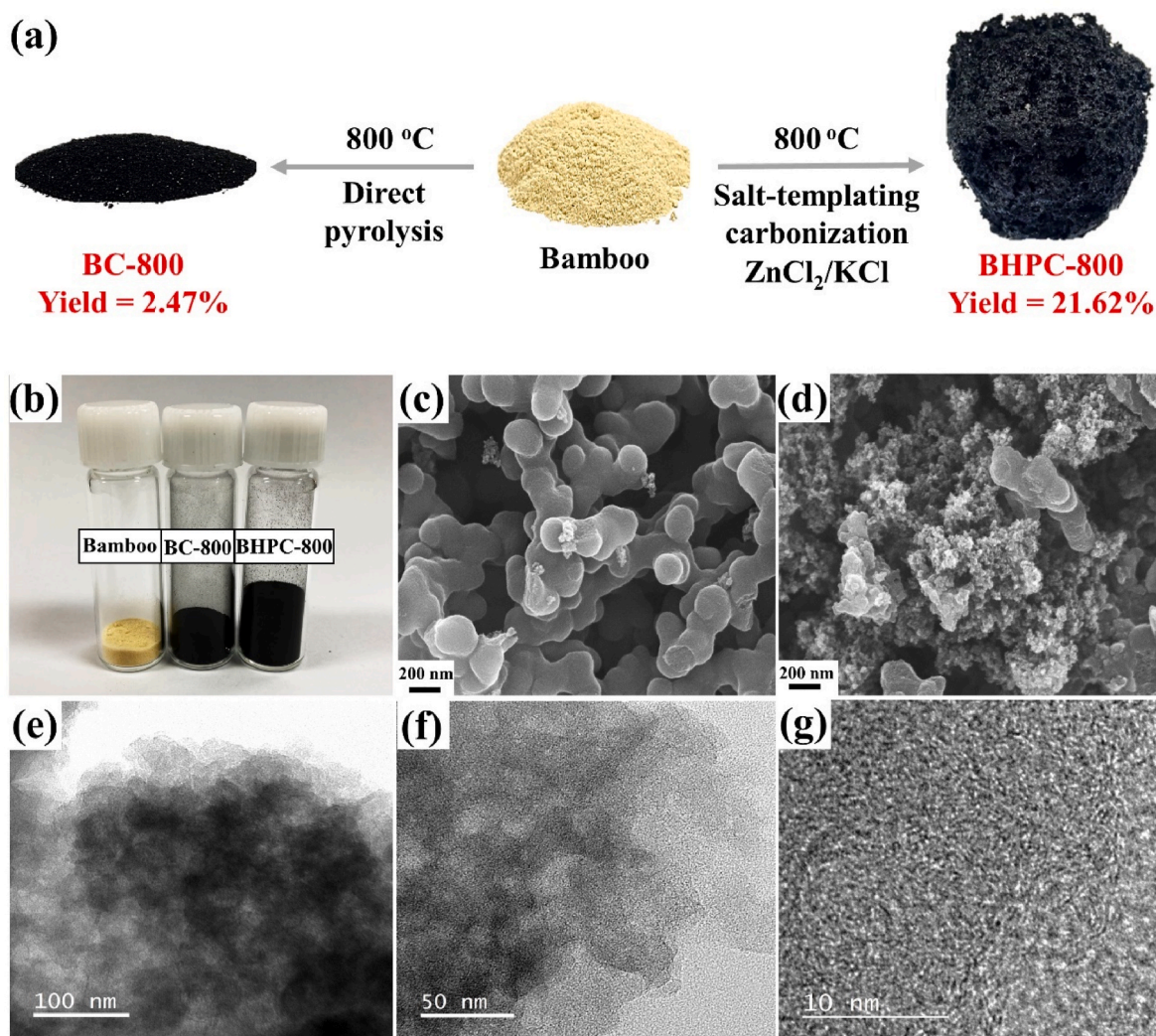

Fig. 1. (a) Preparation of bamboo charcoal (BC-800) and bamboo-derived hierarchical porous carbon (BHPC-800); (b) Macroscopic volume of the as-prepared samples (100 mg each); SEM images of (c) BC-800 and (d) BHPC-800; and (e–g) TEM images of BHPC-800 at different magnification. (A colour version of this figure can be viewed online.)

structure and undeveloped porosity. The residual carbon material was arranged in an irregular manner without structure-directing agents, leaving free volumes that may be occupied by disorganized carbon, resulting in the contraction/collapse of the carbon framework. The porous structure of the resulting char was then largely restricted, leading to the formation of undeveloped porosity. Therefore, the formation of condensed and undeveloped porous char resulted in a very low carbon yield of 2.47%. In contrast, the product from the carbonization under the presence of the salt mixture (BHPC-800) demonstrated a 3D hierarchical porous structure with highly-developed interconnected framework and the carbon yield of 21.62%. Moreover, BHPC-800 showed higher macroscopic volume in comparison with BC-800, and yet significantly larger than bamboo (Fig. 1b). As shown in Fig. 1c, SEM image of BC-800 indicates the condensed particles and it is impossible to see the porous structure, however, the porosity of BHPC-800 is easily observed in the micrograph (Fig. 1d). This phenomenon could be explained by the fact that the salt mixture infiltrated to the carbon structure during the carbonization, impeding the compaction/disappearance of the pore systems that caused the volume shrinkage and promoting the formation of well-developed porous carbon with the increased carbon yield. TEM characterization was further accessed to elaborate the porous feature of the BHPC samples. As shown in Fig. 1e and f, BHPC-800 is composed of abundant mesopores and macropores in the carbon framework. Moreover, the high-resolution TEM image (Fig. 1g) displays large amounts of light and dark spots, further confirming the presence of high-density micropores.

The formation mechanism of porous structure in the presence of the salt mixture could be considered as a templating method. During the carbonization process, the homogenous mixture of the carbon precursor and the salts was heated up to 250 °C and kept for 2 h and the salt mixture started to melt. At this stage, the melting salt mixture accelerated the dehydration reactions that may cause the compaction of the

carbon framework. Such compaction was partially prohibited due to the presence of the reactants throughout the carbonization process. Thus, the salt molecules and their hydrates remaining inside the carbon particles acted as molecular templates for the formation of mainly micropores. The opening of interconnected meso- and macroporosity could be adjusted by varying the salt to precursor ratios. At the fixed ratio of bamboo to the salt mixture (1/10, wt/wt), the melted salts could create larger salt clusters leading to the phase separation of the carbon phase and the salt phase. The larger salt domains defined the greater pore size and pore structure. When the carbonization process came to a suitable temperature, the reaction mixture was cooled down to room temperature and the salt clusters were allowed to solidify. After removing the salts through aqueous washing process, the hierarchical pores of the resulting carbon product were formed. These above-mentioned results give evidence about the synergistic role of the salts not only in the prevention of the material from collapse/decomposition but also in the development of porous structure during the carbonization process.

To further investigate the role of the salt mixture, TGA profiles were evaluated for the bamboo, the salt mixture, and the bamboo mixed with the salts at the mass ratio of 1:10. As shown in Fig. 2a, the TG curve of bamboo demonstrates that bamboo started its weight loss at around 200 °C and most of the material lost its weight at 500 °C. This indicates that the pyrolysis process of the biomass mainly took place in the temperature range of 200–500 °C. Particularly, the decomposition of bamboo under air atmosphere indicates two weight loss stages. The first weight loss (200−365 °C) is the main thermal decomposition of bamboo, while the second weight loss (365−500 °C) attributes to the evaporation of volatiles and the combustion of the charred product [23]. Moreover, it is evident that bamboo completely burned, resulting a very low weight loss of approximately 4% at 800 °C. As a contrast, the salt mixture began its weight loss at 500 °C, corresponding to the evaporation of the salt mixture. The TG curve of bamboo/salt mixture also
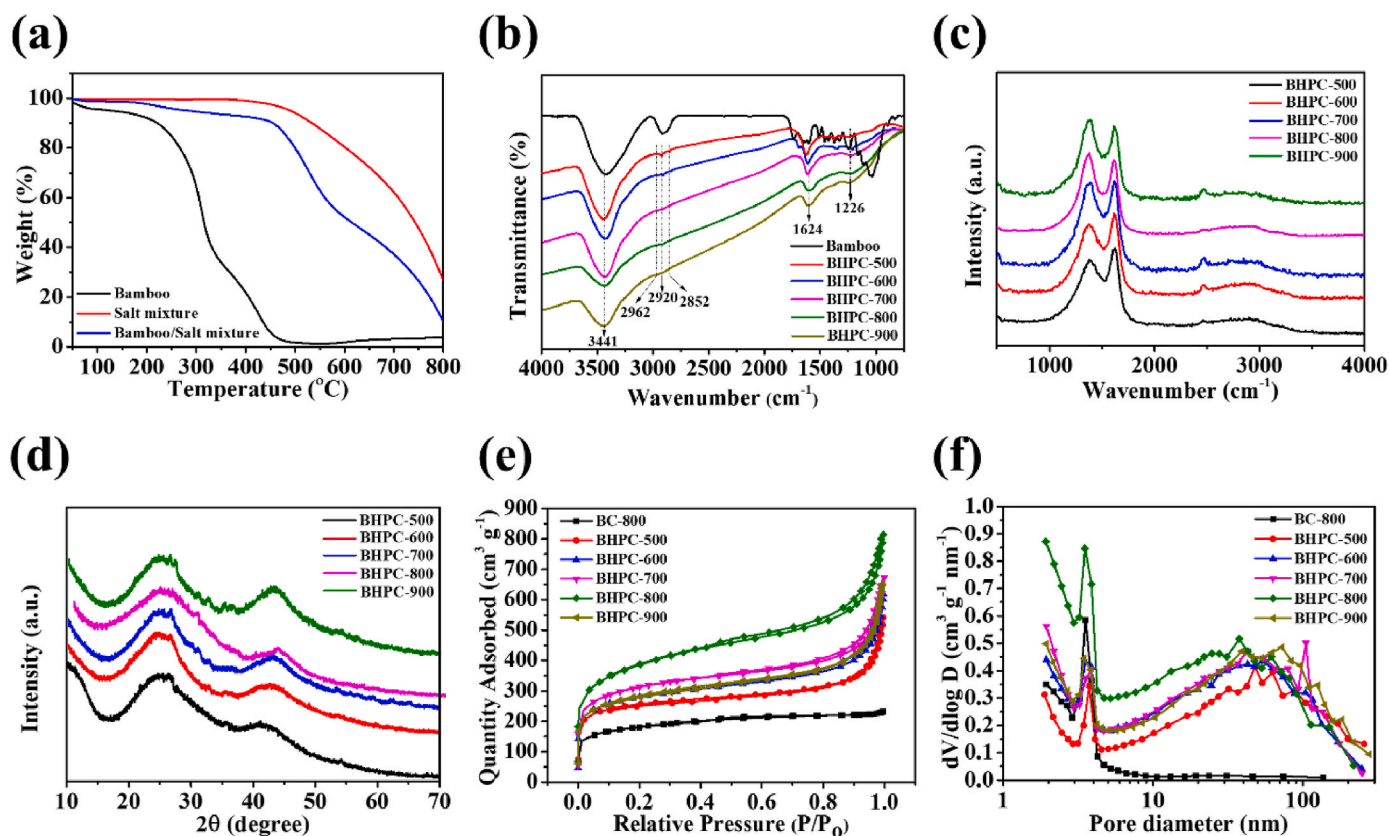

Fig. 2. (a) TGA diagrams of bamboo, salt mixture, and bamboo/salt mixture; (b) FTIR spectra; (c) Raman spectra; (d) XRD patterns; (e) Nitrogen adsorption/desorption isotherms; and (f) BJH pore size distributions of all the carbon samples. (A colour version of this figure can be viewed online.)

exhibits two weight loss stages. However, the first weight loss occurred in the temperature range of 200–500 °C only with the 5 wt% weight loss. The salt mixture is considered acting as a shielding agent at this stage, restricting the material from burning. It is worth noting that the addition of the salts resulted in the shift of second weight loss stages in the TG curve of bamboo/salt mixture towards higher temperature. Therefore, the main carbonization process of the biomass occurred at higher temperature above 500 °C, according to the TG curve of bamboo/salt mixture. When the temperature was elevated to 800 °C, the weight loss of around 10 wt% was obtained, which is higher than that of the biomass without the salt protection.

The carbonization process progressively occurred through the steady transition from sp^3 C–X (X = C, O, H) bonds to aromatic sp^2 C=C bonds during the conversion of bamboo into carbon materials. The conversion of the sp^3 C – X bonds of bamboo into the sp^2 C=C bonds was further examined by several spectroscopic techniques. As seen in Fig. 2b, the FTIR spectrum of bamboo shows various peaks of different functional groups in the material (Table S1). The intensities of these peaks were reduced at higher carbonization temperatures. The samples obtained at low temperatures (T < 600 °C) exhibited the peaks indicating the presence of the O–H stretching (3441 cm^{-1}), the C–H stretching (2962, 2920, and 2852 cm^{-1}), the C=O stretching (1710 cm^{-1}), the O–H bending (1375 cm^{-1}), and the C–O stretching (1226 and 1083 cm^{-1}). The existence of sp^2 bonded benzene rings is also clear in the vibrational regions of 1624 cm^{-1} (the C=C stretching) and 894 cm^{-1} (the C–H stretching) [24]. For the samples obtained at high carbonization temperatures (T > 600 °C), the FTIR curves became smooth, and the intensities of the O–H, C–H, C=C, and C–O groups decreased significantly, resulting from the strong absorption of the sp^2 bonded carbon in the infrared region.

The structural characteristic of the carbon samples was further investigated by Raman spectroscopy. As shown in Fig. 2c, it is worth noting that all the samples displayed two broad and overlapping peaks at 1341 and 1590 cm^{-1}, corresponding to the D-band (disordered and defect structure) and G-band (graphitic structure) of the carbon material, respectively [25]. Carbonization at different temperatures is considered to cause the changes in the material structure, leading to a slight enhancement in the intensity of the D band of the samples. The higher I_D/I_G values indicate that the as-formed carbon materials could be considered as disordered graphitic structures. The XRD spectra in Fig. 2d show that all the samples exhibited two broad peaks located at 26 ° and 43 °, which are typical characteristics of the (002) and (100) planes of graphitic carbon [26]. This indicates that the salt-aided carbonization at high temperature triggered the formation of amorphous structure with a limited degree of graphitization, which are consistent with the Raman analysis.

The nitrogen adsorption/desorption experiments were conducted to investigate the hierarchical porous structure generating mechanism of the salt mixture. The associated BET isotherms and BJH pore size distributions of the obtained carbon samples are shown in Fig. 2e and f, respectively. From the quantitative analysis of nitrogen adsorption/desorption isotherms (Fig. 2e), the obtained BC-800 sample, which was made through direct carbonization without the use of salt mixture displayed a typical type-I isotherm curve and the lowest gas adsorption, indicating the undeveloped porosity. On the contrary, all BHPC samples exhibit the combined feature of type I and type IV isotherms, in which the significant increase in nitrogen adsorption at low relative pressure region (P/P$_0$ < 0.1) indicates the formation of enriched micropores; the small hysteresis loops observed in the moderate relative pressure are the characteristics for the existence of mesopores; the rapid increase at P/P$_0$ > 0.9 suggests the development of macropores in the samples [27]. Consequently, the results illustrate that the carbonization with the utilization of the salt mixture induced the generation of hierarchical porous carbon structures. In addition, the specific surface area, pore volume, and pore size distribution of the carbon samples are summarized in Table 1. The directly pyrolyzed sample (BC-800) shows a relatively low

Table 1

Pore properties obtained from nitrogen adsorption/desorption results of the as-prepared materials.

Samples	^{a}SSA (m^2 g^{-1})	^{b}TPV (cm^3 g^{-1})	^{c}V$_{mic}$ (cm^3 g^{-1})	^{d}%V$_{mic}$	^{e}PSD (nm)
BC-800	600	0.36	0.14	38.89	2.39
BHPC-500	827	0.83	0.26	31.33	4.03
BHPC-600	917	0.95	0.24	25.26	4.16
BHPC-700	1029	1.03	0.25	24.27	4.00
BHPC-800	1296	1.26	0.23	18.25	3.88
BHPC-900	930	1.01	0.21	20.79	4.35

^{a} SSA: specific surface area calculated from the adsorption data by BET method.
^{b} TPV: total pore volume calculated from the adsorption data at P/P$_0$ = 0.995.
^{c} V$_{mic}$: micropore volume calculated by t-plot method.
^{d} %V$_{mic}$: V$_{mic}$/TPV percentage.
^{e} PSD: average pore size distribution estimated from the adsorption data by PSD = 4TPV/SSA.

SSA of 600 m^2 g^{-1} and a limited TPV of 0.36 cm^3 g^{-1}. Such low SSA and TPV are the results of the undeveloped porosity. However, with the use of the salts, the BHPC samples achieved significantly higher SSA and TPV values compared to the BC-800 sample. In detail, BHPC-800 possessed the highest SSA of 1296 m^2 g^{-1} and TPV of 1.26 cm^3 g^{-1}, which was slightly larger than 1029 m^2 g^{-1} and 1.03 cm^3 g^{-1} for BHPC-700, and 930 m^2 g^{-1} and 1.01 cm^3 g^{-1} for BHPC-900; but moderately higher than 917 m^2 g^{-1} and 0.95 cm^3 g^{-1} for BHPC-600, and 827 m^2 g^{-1} and 0.83 cm^3 g^{-1} for BHPC-500. For comparison, at the same temperature of 800 °C, the samples with and without the salts (BC-800 and BHPC-800) indicated a very big difference in the specific surface area and pore properties (Table 1). The effect of the salt mixture on the development of porosity is further investigated via BJH pore size distribution. BC-800 exhibits the combination of micropores (<2 nm) and mesopores (2−50 nm), and no obvious peaks of macropores (>50 nm) could be observed in the plot. On the contrary, BHPC samples have more distributive peaks at 2−50 and 50−300 nm, belonging to mesopores and larger macropores in comparison with the directly pyrolyzed sample. With the increase in carbonization temperature, the pore characteristics of BHPC samples indicated no obvious differences in the pore volume and pore size. As summarized in Table 1, the percentage of micropores (%V$_{mic}$) relatively decreased when the temperature was elevated from 500 to 900 °C, corresponding to the increase in the proportions of mesopores and macropores in all the carbon samples. Moreover, the average PSD of BC-800 achieved a very low value of 2.39 nm, while the BHPCs samples showed the increased PSD values. This slightly increase in the PSD values can be attributed to the opening of pores with larger size. These results imply that the salt-templating carbonization plays a vital role in generating pores with highly developed hierarchical textures. From the porosity analysis, BHPC-700, BHPC-800, and BHPC-900 samples with superior pore characteristics were chosen for further investigation and experiment.

The XPS was performed to investigate the surface chemical compositions of the obtained carbon materials. The XPS spectra in Fig. 3a indicate that all the samples display a strong peak at 284 eV and a small peak at 533 eV, corresponding to C1s and O1s, respectively. The detailed surface chemical composition of all the samples is listed in Table S2. BHPC-700 contains 93.86 at% carbon and 6.14 at% oxygen, while BHPC-800 has 94.78 at% carbon and 5.22 at% oxygen; and C and O contents of BHPC-900 are 95.01 at% and 4.99 at%. As shown in Fig. 3b and Figs. S1a and b, the high-resolution C1s spectra of all the BHPC samples could be deconvoluted into three peaks, including C=C/C–C (284.8 eV), C–O (285.6 eV), and C=O (289.1 eV). Generally, as the carbonization temperature increasing, the content of C=C/C–C tends to increase, while the contents of C–O and C=O seem to decrease (Table S3). This may be due to the burning of the carbonized products. The elemental percentages of C species show no distinguishable
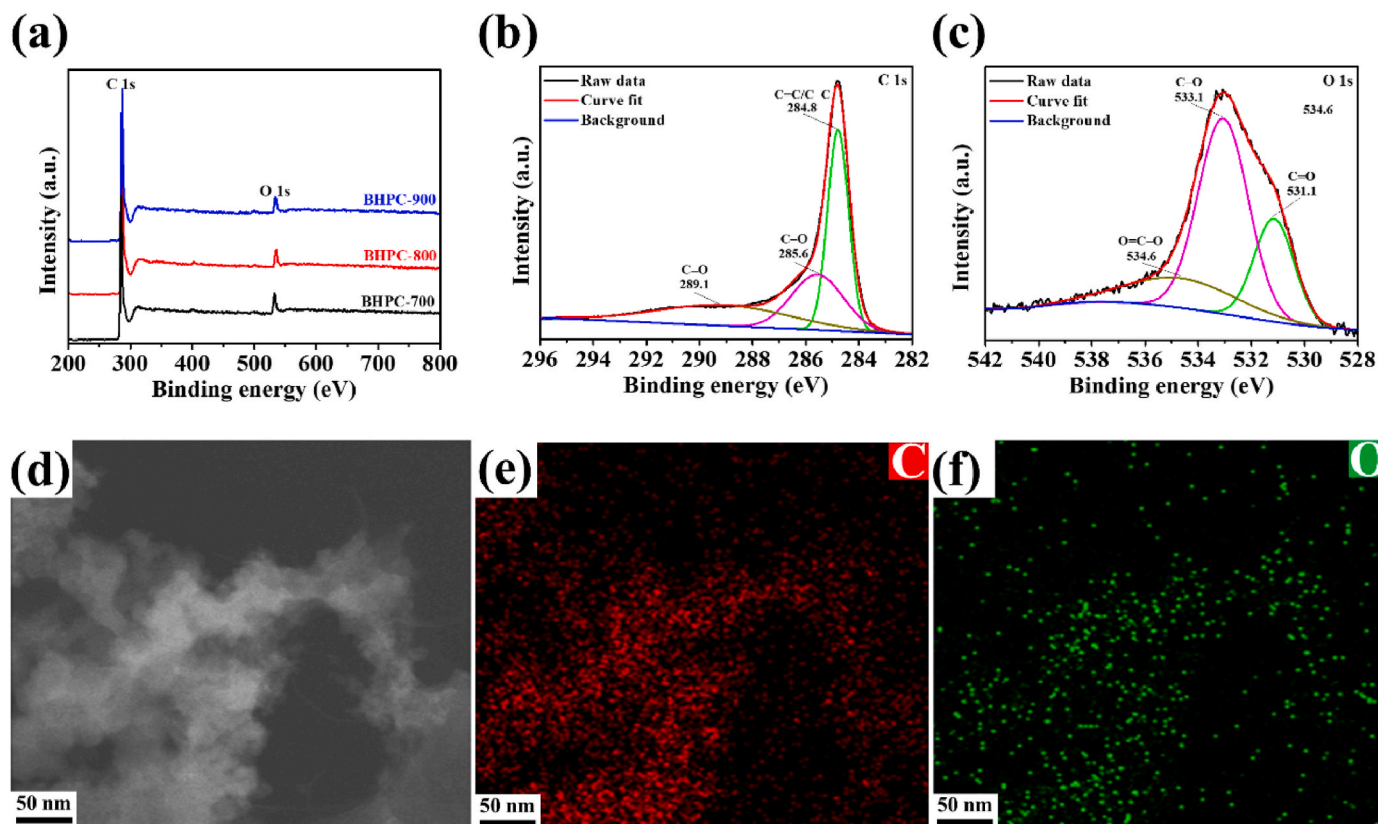
Fig. 3. (a) XPS survey spectra; high-resolution XPS spectra of (b) C1s and (c) O1s of BHPC-800; (d) TEM image and (e, f) elemental mapping images of BHPC-800. (A colour version of this figure can be viewed online.)

difference. However, the carbonization temperature affected the elemental percentages of heteroatom. The O1s spectra in Fig. 3c and Figs. S1c and d could be distinguished into three peaks, including C=O (531.1 eV), C–O (533.1 eV), and O=C–O (534.6 eV). There is a decrease in the contents of all oxygen functional groups as carbonization temperature increasing, particularly for O=C–O, which significantly decreases at high temperature. At 900 °C, the content of C–O–C tends to increase, which may be due to dehydration reactions between adjacent hydroxyl molecules. Moreover, the raise of C=O may result from the addition reaction between C=C and gaseous CO [28]. Typically, these oxygenated functional groups not only can enhance surface wettability of the carbon materials but also can contribute to the overall capacitance by inducing additional pseudo-capacitance. Elemental distribution of the BHPCs samples were analyzed by TEM Energy-dispersive X-ray Spectroscopy (EDS), as shown in Fig. 3e and f. The results reveal that carbon and oxygen elements are homogeneously distributed in the carbon skeletons.

3.2. Electrochemical performance in three-electrode system

The electrochemical performances of BHPC-700, BHPC-800, and BHPC-900 were evaluated in the three-electrode system using a 6 M KOH aqueous electrolyte. Fig. 4a presents the CV curves of the BHPC samples at a scan rate of 50 mV s^{-1}. The typical CV profiles of the BHPC-700, BHPC-800, and BHPC-900 electrodes exhibit quasi-rectangular shapes with equivalent current responses during the positive and negative voltage scans, resulting from the electrostatic charge accumulation at the electrode/electrolyte interface. In addition, slight Faraday humps observed in all the samples attribute to the pseudo-capacitance behavior, which is due to the oxygen-containing groups. Furthermore, BHPC-800 and BHPC-900 also show more obvious redox peaks between −0.4 and −0.1 V compared to that of BHPC-700. The contribution of

pseudo-capacitance to the overall capacitance of the BHPC electrodes comes from the Faraday redox reactions of the hydroxyl, carboxyl, and phenolic groups of oxygen in the alkaline electrolyte [29]. The CV results imply that the ideal capacitive nature of the as-prepared carbon electrodes benefits from the combination of favorable electric double layer capacitance (EDLC) and pseudo-capacitance (PC) behaviors. In fact, the BHPC-800 displays the largest current response in the CV curve in comparison with the other two samples, resulting in its highest capacitive characteristics. In consistent with the CV outcomes, the GCD curves of all the samples at a current density of 1 A g^{-1} (Fig. 4b) present triangular shapes, and BHPC-800 shows the longest charge/discharge time, indicating its excellent capacitive behaviors. Calculated from the GCD curves, the specific capacitance of BHPC-800 is 394 F g^{-1}, which is higher than those of the BHPC-700 (307 F g^{-1}) and BHPC-900 (349 F g^{-1}). Moreover, the obtained specific capacitance of the BHPC-800 electrode is remarkably higher compared to those of many reported biomass-derived porous carbonaceous materials (Table S4). Additionally, BHPC-800 electrode shows the best CV and GCD performances than that of the other two electrodes, which should be originated from its highest SSA, largest TPV, an optimum synergistic effect of different pore textures, and suitable heteroatom doping. Increasing the sweep rates from 10 to 200 mV s^{-1} leads to an enlargement of the voltammetric charge area in the CV curves. This observed phenomenon can be explained by the fact that faster scan rate facilitates high adsorption of charges, corresponding to high current response and thus resulting in larger CV profiles [30]. Particularly, the CV curves of the BHPC-800 still retain quasi-rectangular shapes without any distortions, even at a high scan rate of 200 mV s^{-1} (Fig. 4c). The corresponding GCD curves of the BHPC-800 at different current densities from 1 A g^{-1} to 20 A g^{-1} in Fig. 4d exhibit almost symmetrical linear, indicating that the BHPC-800 still has the properties of double-layer capacitance and favorable electrochemical reversibility. The specific capacitance values calculated at
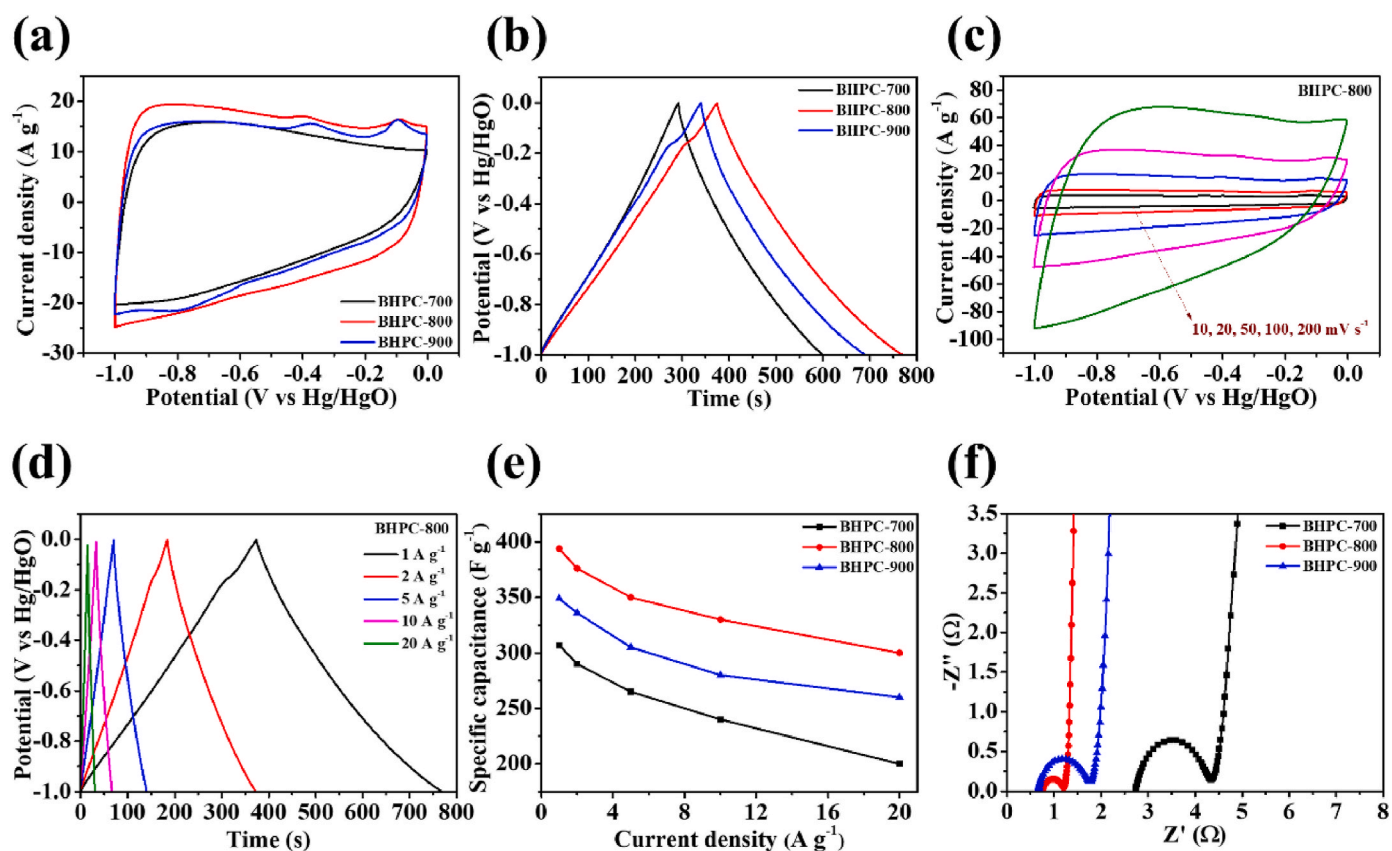
Fig. 4. Electrochemical performance of the as-prepared carbon electrodes in a three-electrode system in a 6 M KOH aqueous electrolyte. (a) CV curves of BHPC-700, BHPC-800, and BHPC-900 at 50 mV s^{-1}; (b) GCD curves of BHPC-700, BHPC-800, and BHPC-900 at 1 A g^{-1}; (c) CV curves of BHPC-800 at different scan rates; (d) GCD curves of BHPC-800 at different current densities; (e) Specific capacitance of BHPC-700, BHPC-800, and BHPC-900 at different current densities; and (f) Nyquist plots of BHPC-700, BHPC-800, and BHPC-900. (A colour version of this figure can be viewed online.)

different current densities were further used to access the rate capacity of the as-prepared BHPC electrodes. As shown in Fig. 4e, the BHPC-800 electrode still offered high specific capacitance of 300 F g^{-1} even at high current density of 20 A g^{-1}, compared to those of 200 F g^{-1} (BHPC-700) and 260 F g^{-1} (BHPC-900). Notably, the capacitance retention of the BHPC-800 electrode remained at 76.14% of initial capacitance (394 F g^{-1}) when the current density was increased from 1 to 20 A g^{-1}, further confirming the good rate performance of the BHPC-800 electrode. The detailed CV and GCD curves of the BHPC-700 and BHPC-900 are shown in Fig. S2.

The electrochemical impedance spectroscopy (EIS) was recorded to further investigate the electrochemical properties of the carbon samples. Typical Nyquist plots of all the as-prepared electrodes in Fig. 4f indicate two regions, including a semicircle at high frequency region followed by a straight line at low frequency region. It is well accepted that the first intersection of the Nyquist plot and the Z' axis in the high frequency region is indicative of the solution resistance (R$_s$) involving the intrinsic resistance of electrode material, ionic resistance of electrolyte, and contact resistance between the electrode and current collector. The diameter of the semicircle in the high frequency region is attributable to the charge transfer resistance (R$_{ct}$) at the electrolyte and electrode interface, while the slope of the straight line is characteristic of Warburg resistance (Z$_W$) [30]. As summarized in Table S5, the R$_s$ and R$_{ct}$ values of BHPC-800 are 0.76 and 0.44 Ω, respectively, indicating the relatively low solution resistance and the smallest charge transfer resistance compared to the other as-prepared electrode materials. Such the low R$_s$ value and smallest semicircle diameter of BHPC-800 demonstrate an excellent electrical conductivity and a rapid charge transfer of the electrolyte ions. Moreover, the nearly approached vertical line of BHPC-800 in the low frequency region also shows a clear indication of

fast ion diffusion and ideal capacitive behavior. Consequently, all the CV, GCD, and EIS results clearly state that BHPC-800 displays remarkable electrochemical performances in three-electrode system as compared to the other samples. It is considered because the BHPC-800 offers the highest specific surface area, pore volume, and a set number of pore size distributions, providing accessible sites for ions to penetrate, diffuse and transport during charge/discharge process. More specifically, the hierarchical porous structure containing micro-, meso-, and macropores at various length scales in the carbon material demonstrates the synergistic effect in favor of enhancing the electrochemical performances of the active materials. The micropores facilitate the formation of enriched active sites, which are most effective in improving double-layer capacitance. Meanwhile, the interconnected mesopores offer low-resistance channels for accelerating ions diffusion and transport. The macropores play a role as ion buffering reservoirs decreasing the ion transportation distance from electrolyte [31]. Moreover, the incorporation of oxygen-containing groups in the porous carbon can facilitate wetting ability between electrode and electrolyte, thus increasing ions penetration, and promoting pseudo-capacitance.

3.3. Electrochemical performance of the symmetric supercapacitor in aqueous electrolyte

To further examine the electrochemical performance of the as-prepared carbon materials, a symmetric supercapacitor was fabricated by assembling two pieces of the BHPC-800 electrode and tested in the two-electrode system in 6 M KOH aqueous electrolyte. As shown in Fig. 5a, the CV curves of the BHPC-800 symmetric supercapacitor indicate nearly rectangular shapes without any distortion even at high scan rate of 200 mV s^{-1}, indicating its good reversible property and good
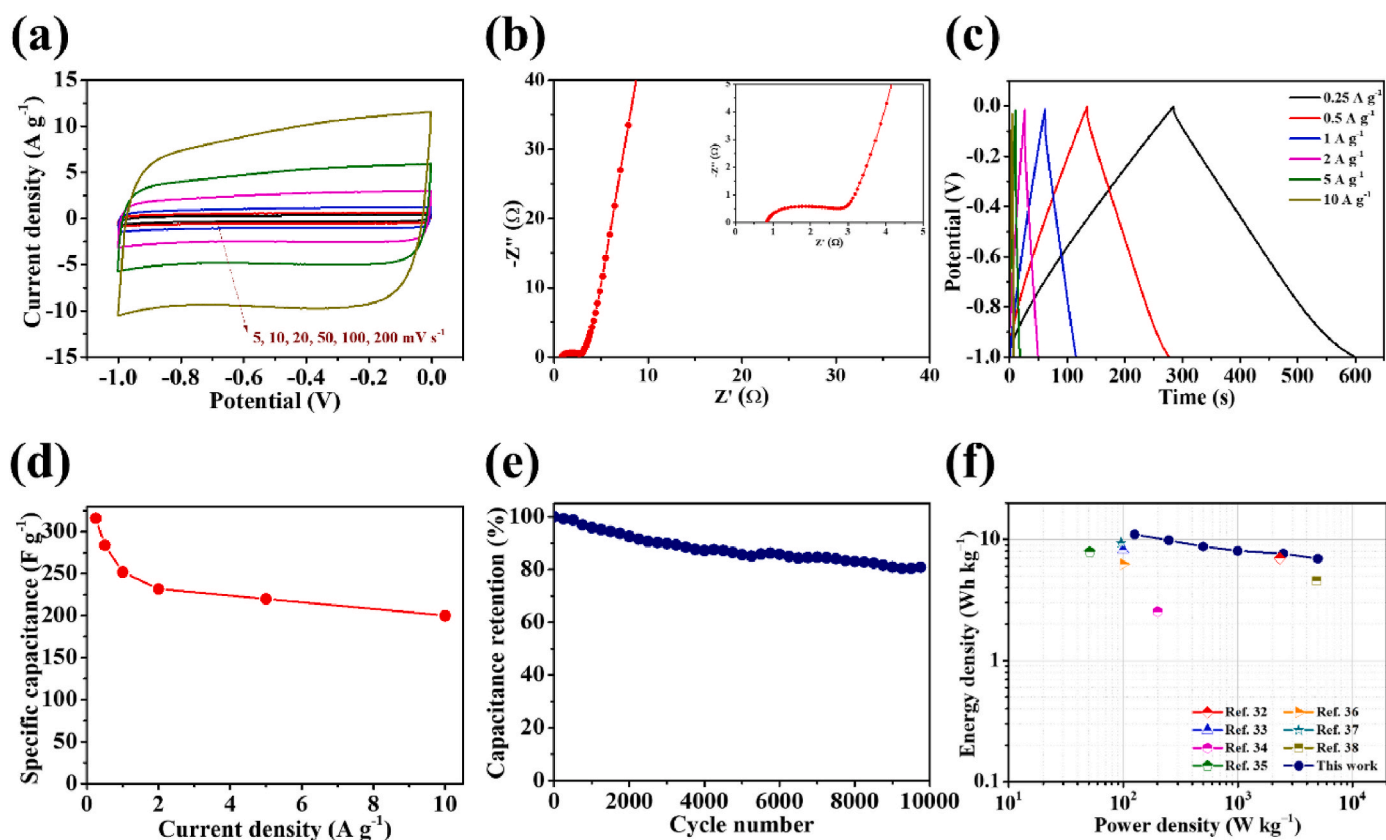
Fig. 5. Electrochemical performance of the as-prepared symmetric supercapacitor based on the BHPC-800 electrode in a 6 M KOH aqueous electrolyte. (a) CV curves at different scan rates; (b) Nyquist plots; (c) GCD curves at different current density; (d) Specific capacitance at different current density; (e) Stability test conducted at 1 A g^{-1} for 10,000 cycles; and (f) Ragone plots of symmetric supercapacitor in a 6 M KOH aqueous electrolyte. (A colour version of this figure can be viewed online.)

rate performance. The EIS spectra in Fig. 5b were used to access the impedance response of the BHPC-800 symmetric supercapacitor. It was found that the Nyquist plot has a relatively small R_s (0.84 Ω), a small semicircle in the high-frequency corresponding to a low R_{ct} (1.89 Ω), combined with a non-vertical line in the low-frequency region. The results demonstrate the good conductivity and fast ion diffusion and transport of the device in aqueous electrolyte. The GCD profiles of the BHPC-800 symmetric supercapacitor (Fig. 5c) still keep in the shape of symmetric triangles, indicating its outstanding EDLC behaviors. Calculated from the GCD curves, the BHPC-800 symmetric supercapacitor delivers the specific capacitances of 316, 284, 252, 232, 220, and 200 F g^{-1} under current densities of 0.25, 0.5, 1, 2, 5, and 10 A g^{-1}, respectively. It is worth noting that the capacitance retention of 63.29% at high current density of 10 A g^{-1} further confirms the good rate capability of the device (Fig. 5d).

Stability performance is one of the main requirements for the practical application of the supercapacitor. As shown in Fig. 5e, cycle life of the BHPC-800 symmetric supercapacitor tested at 1 A g^{-1} demonstrates that the capacitance retention of 81% over 10,000 cycles of continuous charge-discharge process was obtained, confirming long-term cyclic stability of the device. Energy density and power density are also crucial parameters for the final performance of the supercapacitor. Ragone plot in Fig. 5f indicates that an energy density of 11 Wh kg^{-1} could be acquired at a power density of 126 W kg^{-1} and the energy density remains 7 Wh kg^{-1} even at high power density of 5000 W kg^{-1}, which is superior to those of commercial active carbon and other biomass carbon-based symmetric supercapacitors previously reported in the literature [32–38]. The above demonstrations further proved that the as-synthesized bamboo-derived hierarchical porous carbon could be considered as a promising candidate in energy storage and conversion

field.

4. Conclusion

In this work, a new hierarchical porous carbon derived from a readily available and sustainable bamboo as the precursor using a green and scalable ZnCl$_2$/KCl salt-templating strategy was reported. This technique was conducted under the air atmosphere avoiding the utilization of complex equipment and inert gas environment, which is more feasible and easier to scale up. The as-prepared materials possess a 3D interconnected porous network with excellent characteristics consisting of abundant micro-meso-macropores, large specific surface area, and large total pore volume. The optimal sample (BHPC-800) as the electrode material for supercapacitor displays an outstanding specific capacitance of 394 F g^{-1} at 1 A g^{-1} in a three-electrode system. Moreover, the symmetric BHPC-800 supercapacitor also exhibits a high specific capacitance of 316 F g^{-1} at 0.25 A g^{-1}, a good rate capability, and a stable cycle life. Moreover, the as-prepared device delivers a high energy density of 11 Wh kg^{-1} at 126 W kg^{-1} in an aqueous electrolyte. Importantly, the concept of preparing high-value electrode materials from a cheap and renewable carbon source is expected to offer a new opportunity for future studies on the modification of porous carbon materials (i.e., heteroatom doping, incorporation of conductive polymer, graphene, metal oxides, etc.) for wide-range energy conversion and storage applications.

CRediT authorship contribution statement

Tan Binh Nguyen: Conceptualization, Methodology, Formal analysis, Investigation, Writing – original draft, Writing – review & editing.

Bumyong Yoon: Writing – review & editing. **Trong Danh Nguyen:** Resources. **Eunyoung Oh:** Resources. **Yifei Ma:** Resources. **Mei Wang:** Writing – review & editing. **Jonghwan Suhr:** Writing – review & editing, Data curation, Funding acquisition, Project administration, Supervision.

Declaration of competing interest

The authors declare that they have no known competing financial interests or personal relationships that could have appeared to influence the work reported in this paper.

Acknowledgements

Appendix A. Supplementary data

Supplementary data to this article can be found online at https://doi. org/10.1016/j.carbon.2023.02.060.

References

[1] H. Jin, J. Li, Y. Yuan, J. Wang, J. Lu, S. Wang, Recent progress in biomass-derived electrode materials for high volumetric performance supercapacitors, Adv. Energy Mater. 8 (2018), 1801007, https://doi.org/10.1002/aenm.201801007.

[2] Q. Wang, J. Yan, Z. Fan, Carbon materials for high volumetric performance supercapacitors: design, progress, challenges, and opportunities, Energy Environ. Sci. 9 (2016) 729–762, https://doi.org/10.1039/C5EE03109E.

[3] X. Chen, C. Li, M. Grätzel, R. Kostecki, S.S. Mao, Nanomaterials for renewable energy production and storage, Chem. Soc. Rev. 41 (2012) 7909–7937, https://doi.org/10.1039/C2CS35230C.

[4] G. Wang, L. Zhang, J. Zhang, A review of electrode materials for electrochemical supercapacitors, Chem. Soc. Rev. 41 (2012) 797–828, https://doi.org/10.1039/C1CS15060J.

[5] J. Wang, X. Zhang, Z. Li, Y. Ma, L. Ma, Recent progress of biomass-derived carbon materials for supercapacitors, J. Power Sources 451 (2020), 227794, https://doi.org/10.1016/j.jpowsour.2020.227794.

[6] Z. Yu, L. Tetard, L. Zhai, J. Thomas, Supercapacitor electrode materials: nanostructures from 0 to 3 dimensions, Energy Environ. Sci. 8 (2015) 702–730, https://doi.org/10.1039/C4EE03229B.

[7] C. Li, X. Zhang, K. Wang, X. Sun, G. Liu, J. Li, H. Tian, J. Li, Y. Ma, Scalable self-propagating high-temperature synthesis of graphene for supercapacitors with superior power density and cyclic stability, Adv. Mater. 29 (2017), 1604690, https://doi.org/10.1002/adma.201604690.

[8] J. Zhou, S. Zhang, Y.-N. Zhou, W. Tang, J. Yang, C. Peng, Z. Guo, Biomass-derived carbon materials for high-performance supercapacitors: current status and perspective, Electrochem. Energ. Rev. 4 (2021) 219–248, https://doi.org/10.1007/s41918-020-00090-3.

[9] Y. Zhang, X. Liu, S. Wang, L. Li, S. Dou, Bio-Nanotechnology in high-performance supercapacitors, Adv. Energy Mater. 7 (2017) 1700592, https://doi.org/10.1002/aenm.201700592.

[10] F. Béguin, V. Presser, A. Balducci, E. Frackowiak, Carbons and electrolytes for advanced supercapacitors, Adv. Mater. 26 (2014) 2219–2251, https://doi.org/10.1002/adma.201304137.

[11] Z. Bi, Q. Kong, Y. Cao, G. Sun, F. Su, X. Wei, X. Li, A. Ahmad, L. Xie, C.-M. Chen, Biomass-derived porous carbon materials with different dimensions for supercapacitor electrodes: a review, J. Mater. Chem. 7 (2019), 16028, https://doi.org/10.1039/C9TA04436A.

[12] J. Zhang, J. Li, D. Ye, X. Zhu, Q. Liao, B. Zhang, Tubular bamboo charcoal for anode in microbial fuel cells, J. Power Sources 272 (2014) 277–282, https://doi.org/10.1016/j.jpowsour.2014.08.115.

[13] P. Liao, Z.M. Ismael, W. Zhang, S. Yuan, M. Tong, K. Wang, J. Bao, Adsorption of dyes from aqueous solutions by microwave modified bamboo charcoal, Chem. Eng. J. 195–196 (2012) 339–346, https://doi.org/10.1016/j.cej.2012.04.092.

[14] F.Y. Wang, H. Wang, J.W. Ma, Adsorption of cadmium (II) ions from aqueous solution by a new low-cost adsorbent–Bamboo charcoal, J. Hazard Mater. 177 (2010) 300–306, https://doi.org/10.1016/j.jhazmat.2009.12.032.

[15] S.-Y. Wang, M.-H. Tsai, S.-F. Lo, M.-J. Tsai, Effects of manufacturing conditions on the adsorption capacity of heavy metal ions by Makino bamboo charcoal, Bioresour. Technol. 99 (2008) 7027–7033, https://doi.org/10.1016/j.biortech.2008.01.014.

[16] K.H. Wu, T.H. Ting, C.I. Liu, C.C. Yang, J.S. Hsu, Electromagnetic and microwave absorbing properties of Ni0.5Zn0.5Fe2O4/bamboo charcoal core–shell nanocomposites, Compos. Sci. Technol. 68 (2008) 132–139, https://doi.org/10.1016/j.compscitech.2007.05.028.

[17] M.-p. Ho, K.-t. Lau, H. Wang, D. Hui, Improvement on the properties of polylactic acid (PLA) using bamboo charcoal particles, Compos. B Eng. 81 (2015) 14–25, https://doi.org/10.1016/j.compositesb.2015.05.048.

[18] W. Nitayaphat, N. Jiratumnukul, S. Charuchinda, S. Kittinaovarat, Mechanical properties of chitosan/bamboo charcoal composite films made with normal and surface oxidized charcoal, Carbohydr. Polym. 78 (2009) 444–448, https://doi.org/10.1016/j.carbpol.2009.04.027.

[19] J. Zhang, J. Zheng, W. Yang, Green supercapacitor assisted photocatalytic fuel cell system for sustainable hydrogen production, Chem. Eng. J. 403 (2021), 1263682, https://doi.org/10.1016/j.cej.2020.126368.

[20] J. Wang, P. Nie, B. Ding, S. Dong, X. Hao, H. Duo, X. Zhang, Biomass derived carbon for energy storage devices, J. Mater. Chem. 5 (2017) 2411–2428, https://doi.org/10.1039/C6TA08742F.

[21] J. Pampel, A. Mehmood, M. Antonietti, T.-P. Fellinger, Ionothermal template transformations for preparation of tubular porous nitrogen doped carbons, Mater. Horiz. 4 (2017), 493501, https://doi.org/10.1039/C6MH00592F.

[22] J. Li, N. Wang, J. Tian, W. Qian, W. Chu, Cross-coupled macro-mesoporous carbon network toward record high energy-power density supercapacitor at 4 V, Adv. Funct. Mater. 28 (2018), 1806153, https://doi.org/10.1002/adfm.201806153.

[23] Y. Zhang, G. Ji, C. Li, X. Wang, A. Li, Templating synthesis of hierarchical porous carbon from heavy residue of tire pyrolysis oil for methylene blue removal, Chem. Eng. J. 390 (2020), 124398, https://doi.org/10.1016/j.cej.2020.124398.

[24] Y.Z.N. Htwe, W.S. Chow, Y. Suda, A.A. Thant, M. Mariatti, Effect of electrolytes and sonication times on the formation of graphene using an electrochemical exfoliation process, Appl. Surf. Sci. 469 (2019) 951–961, https://doi.org/10.1016/j.apsusc.2018.11.029.

[25] M.-J. Kim, J.E. Park, S. Kim, M.S. Lim, A. Jin, O.-H. Kim, M.J. Kim, K.-S. Lee, J. Kim, S.-S. Kim, Y.-H. Cho, Y.-E. Sung, Biomass-derived air cathode materials: pore-controlled S,N-co-doped carbon for fuel cells and metal−air batteries, ACS Catal. 9 (2019) 3389–3398, https://doi.org/10.1021/acscatal.8b03730.

[26] S. Yang, S. Wang, X. Liu, L. Li, Biomass derived interconnected hierarchical micro-meso-macroporous carbon with ultrahigh capacitance for supercapacitors, Carbon 147 (2019) 540–549, https://doi.org/10.1016/j.carbon.2019.03.023.

[27] L. Zheng, B. Tang, X. Dai, T. Xing, Y. Ouyang, Y. Wang, B. Chang, H. Shu, X. Wang, High-yield synthesis of N-rich polymer-derived porous carbon with nanorodlike structure and ultrahigh N-doped content for high-performance supercapacitors, Chem. Eng. J. 399 (2020), 125671, https://doi.org/10.1016/j.cej.2020.125671.

[28] H.S. Yuan, X. Huang, H. Wang, L. Xie, J. Cheng, Q. Kong, G. Sun, C.-M. Chen, Structure evolution of oxygen removal from porous carbon for optimizing supercapacitor performance, J. Energy Chem. 51 (2020) 396–404, https://doi.org/10.1016/j.jechem.2020.04.004.

[29] G. Han, J. Jia, Q. Liu, G. Huang, B. Xing, C. Zhang, Y. Cao, Template-activated bifunctional soluble salt ZnCl2 assisted synthesis of coal-based hierarchical porous carbon for high-performance supercapacitors, Carbon 186 (2022) 380–390, https://doi.org/10.1016/j.carbon.2021.10.042.

[30] K. Aruchamy, K. Dharmalingam, C.W. Lee, D. Mondal, N.S. Kotrappanavar, Creating ultrahigh surface area functional carbon from biomass for high performance supercapacitor and facile removal of emerging pollutants, Chem. Eng. J. 427 (2022), 131477, https://doi.org/10.1016/j.cej.2021.131477.

[31] S. Dutta, A. Bhaumik, K.C.-W. Wu, Hierarchically porous carbon derived from polymers and biomass: effect of interconnected pores on energy applications, Energy Environ. Sci. 7 (2014) 3574–3592, https://doi.org/10.1039/C4EE01075B.

[32] S. Song, F. Ma, G. Wu, D. Ma, W. Geng, J. Wan, Facile self-templating large scale preparation of biomass-derived 3D hierarchical porous carbon for advanced supercapacitors, J. Mater. Chem. 3 (2015) 18154–18162, https://doi.org/10.1039/C5TA04721H.

[33] P. Cheng, S. Gao, P. Zang, X. Yang, Y. Bai, H. Xu, Z. Liu, Z. Lei, Hierarchically porous carbon by activation of shiitake mushroom for capacitive energy storage, Carbon 93 (2015) 315–324, https://doi.org/10.1016/j.carbon.2015.05.056.

[34] N. He, S. Yoo, J. Meng, O. yildiz, P.D. Bradford, S. Park, W. Gao, Engineering biorefinery residues from loblolly pine for supercapacitor applications, Carbon 120 (2017) 304–312, https://doi.org/10.1016/j.carbon.2017.05.056.

[35] M. Cao, Q. Wang, W. Cheng, S. Huan, Y. Hu, Z. Liu, C. Han, H. Cheng, G. Wang, A novel strategy combining electrospraying and one-step carbonization for the preparation of ultralight honeycomb-like multilayered carbon from biomass-derived lignin, Carbon 179 (2021) 68–79, https://doi.org/10.1016/j.carbon.2021.03.063.

[36] H. Feng, H. Hu, H. Dong, Y. Xiao, Y. Cai, B. Lei, Y. Liu, M. Zheng, Hierarchical structured carbon derived from bagasse wastes: a simple and efficient synthesis route and its improved electrochemical properties for high-performance supercapacitors, J. Power Sources 302 (2016) 164–173, https://doi.org/10.1016/j.jpowsour.2015.10.063.

[37] Q. Liang, L. Ye, Z.-H. Huang, Q. Xu, Y. Bai, F. Kang, Q.-H. Yang, A honeycomb-like porous carbon derived from pomelo peel for use in high-performance supercapacitors, Nanoscale 6 (2014) 1383–113837, https://doi.org/10.1039/C4NR04541F.

[38] J. Liu, Y. Deng, X. Li, L. Wang, Promising nitrogen-rich porous carbons derived from one-step calcium chloride activation of biomass-based waste for high performance supercapacitors, ACS Sustainable Chem. Eng. 4 (2016) 177–187, https://doi.org/10.1021/acssuschemeng.5b00926.